

## Evaluating the Consistency of Cosmological Distances Using Supernova Siblings in the Near-Infrared

ARIANNA M. DWOMOH,<sup>1</sup> ERIK R. PETERSON,<sup>1</sup> DANIEL SCOLNIC,<sup>1</sup> CHRIS ASHALL,<sup>2</sup> JAMES M. DERKACY,<sup>2</sup> AARON DO,<sup>3</sup>  
JOEL JOHANSSON,<sup>4</sup> DAVID O. JONES,<sup>5</sup> ADAM G. RIESS,<sup>6,7</sup> AND BENJAMIN J. SHAPPEE<sup>3</sup>

<sup>1</sup>*Department of Physics, Duke University, Durham, NC 27708, USA*

<sup>2</sup>*Department of Physics, Virginia Tech, Blacksburg, VA 24061, USA*

<sup>3</sup>*Institute for Astronomy, University of Hawai'i at Mānoa, Honolulu, HI 96822, USA*

<sup>4</sup>*Oskar Klein Centre, Department of Physics, Stockholm University, AlbaNova, SE-10691 Stockholm, Sweden*

<sup>5</sup>*Gemini Observatory, NSF's NOIRLab, 670 N. A'ohoku Place, Hilo, HI 96720, USA*

<sup>6</sup>*Space Telescope Science Institute, Baltimore, MD 21218, USA*

<sup>7</sup>*Department of Physics and Astronomy, Johns Hopkins University, Baltimore, MD 21218, USA*

### ABSTRACT

The study of supernova siblings, supernovae with the same host galaxy, is an important avenue for understanding and measuring the properties of Type Ia Supernova (SN Ia) light curves (LCs). Thus far, sibling analyses have mainly focused on optical LC data. Considering that LCs in the near-infrared (NIR) are expected to be better standard candles than those in the optical, we carry out the first analysis compiling SN siblings with only NIR data. We perform an extensive literature search of all SN siblings and find six sets of siblings with published NIR photometry. We calibrate each set of siblings ensuring they are on homogeneous photometric systems, fit the LCs with the SALT3-NIR and SNooPy models, and find median absolute differences in  $\mu$  values between siblings of 0.248 mag and 0.186 mag, respectively. To evaluate the significance of these differences beyond measurement noise, we run simulations that mimic these LCs and provide an estimate for uncertainty on these median absolute differences of  $\sim 0.052$  mag, and we find that, statistically, our analysis rules out the nonexistence of intrinsic scatter in the NIR at the 99% level. When comparing the same sets of SN siblings, we observe a median absolute difference in  $\mu$  values between siblings of 0.177 mag when using optical data alone as compared to 0.186 mag when using NIR data alone. It is unclear if these results may be due to limited statistics or poor quality NIR data; all of which will be improved with the Nancy Grace Roman Space Telescope.

*Keywords:* supernovae: general, cosmology: distance scale

### 1. INTRODUCTION

Type Ia Supernovae (SNe Ia) are used to measure the local expansion rate of the universe (e.g., Freedman et al. 2019; Riess et al. 2022), as well as the expansion history (e.g., Scolnic et al. 2022; Brout et al. 2022). In most SN Ia cosmological analyses, SNe Ia are treated as “standardizable candles” by using light curve (LC) properties to infer an absolute optical luminosity. Still, after standardization, there is an unknown scatter left in luminosity magnitudes, deemed “intrinsic scatter” ( $\sigma_{\text{int}}$ ). One way to better understand  $\sigma_{\text{int}}$  is by analyzing SN “siblings,” SNe found within the same host galaxy. These siblings uncover correlations between SN properties and host galaxy properties (Scolnic et al. 2020; Kelsey 2023). Furthermore, siblings can be studied to help understand the effects from various local environ-

ments within a galaxy. Here, we examine SN siblings, focusing on LCs in the near-infrared (NIR).

There have been a number of SN sibling analyses using optical measurements that reach varying conclusions. Scolnic et al. (2020) use a Dark Energy Survey sample of photometrically-identified SNe Ia to find eight sets of siblings and compare the LC properties of those SNe to their distances. They place an upper limit that, at most, half of the  $\sigma_{\text{int}}$  of the SN Ia Hubble residuals can be attributed to the parent galaxy. Burns et al. (2020) find a much better distance consistency than Scolnic et al. (2020) of 3% in a sample of 12 sets of SN Ia siblings with predominately optical LCs for observations on the same system, though they discard siblings with SWIFT telescope observations. Biswas et al. (2022) study a pair of siblings, found by the Zwicky Transient Facility (Bellm

et al. 2019) just  $0.57''$  apart at  $z = 0.0541$ , where the two SNe Ia have extremely different colors and use this to attempt to constrain the reddening law for SNe Ia. Ward et al. (2022) analyze the SN sibling trio within NGC 3147 and find that the distances to the siblings are consistent with a standard deviation smaller than the total  $\sigma_{\text{int}}$ . Hoogendam et al. (2022) analyze a galaxy with two fast-declining SN Ia siblings and find that the distances derived from the two are consistent.

All previous SN Ia siblings analyses have reported general consistency in distance measurements in the optical, but this remains to be seen in the NIR. There is particular leverage for understanding SN scatter in the NIR with siblings, as SNe are expected to be even more uniform in luminosity in the NIR (Meikle 2000; Krisciunas et al. 2004a; Wood-Vasey et al. 2008; Mandel et al. 2009; Folatelli et al. 2010; Phillips 2012; Barone-Nugent et al. 2012; Avelino et al. 2019; Jones et al. 2022; Peterson et al. 2023). This uniformity is predicted because of the relationship between the optical and NIR light emitted and temperature, as explained in Kasen (2006). As NIR LCs are less sensitive to the reddening by interstellar dust within host galaxies, NIR observations (photometric and spectroscopic alike) can also help to limit the systematic errors currently present in optical data (Brout & Scolnic 2021). In this work, we perform a full literature search investigating all sets of siblings with NIR data that have been published.

In Section 2, we describe our data collection process and our six sets of siblings. In Section 3, we detail the LC fitting process with both the SALT3-NIR and SNooPy models and compare the resulting differences in distances between siblings. In Section 4, we compare results from our analysis to simulated SN Ia data and assess the implications on intrinsic scatter. We further discuss our results and present our conclusions in Section 5.

## 2. DATA SAMPLE

### 2.1. Data Collection

Outside of the Carnegie Supernova Project (CSP; Hamuy et al. 2006), CfA (Wood-Vasey et al. 2008; Friedman et al. 2015), and the Dark Energy,  $H_0$ , and peculiar Velocities using Infrared Light from Supernovae (DEHVILS; Peterson et al. 2023) survey, there are few large samples of publicly available high-quality NIR data. We used existing (optical) sibling analyses in order to construct a list of SNe for which to search for NIR data. Kelsey (2023) has a large sample of siblings compiled, totaling  $>150$  sets of SN siblings. We also searched on

the Transient Name Server<sup>1</sup> for any SNe within  $2'$  of the DEHVILS SNe detailed in Peterson et al. (2023) looking for potential novel pairs of SN siblings not already listed in previous works.

After compiling this list of all SN siblings in the literature, we used it to look for as many siblings with published NIR photometric data as possible. In total, we found six sets that had any NIR photometric coverage for both siblings.

### 2.2. Siblings

The six sets of siblings we analyze in this paper are SN 1980N/1981D/2006dd/2006mr, SN 2002bo/2002cv, SN 2002dj/2021fxy, SN 2007on/2011iv, SN 2011at/2020jgl, and SN 2020sjo/2020zhh. Information on these SN siblings is further detailed in Table 1. For each SN, we list its host galaxy, type, information source, heliocentric redshift from references linked in the NASA/IPAC Extragalactic Database (NED),<sup>2</sup> NIR filter bandpasses used in this analysis, coordinates, Modified Julian Date (MJD) of the time of peak in the optical, and the total data points for the NIR LC. Optical peak MJD values for DEHVILS SNe are given in Peterson et al. (2023) and calculated from fits to ATLAS (Tonry et al. 2018) LCs. We use the peak MJD values from Pantheon+ (Scolnic et al. 2022; Brout et al. 2022) whenever available; otherwise, we use the reported values from the cited papers in Table 1.  $J$ -band images of the host galaxies are displayed in Fig. 1 with the location of each of the siblings indicated as well. Images with a DEHVILS SN in them are template images from the DEHVILS survey (Peterson et al. 2023), and those without a DEHVILS SN are from the Two Micron All Star Survey (2MASS; Skrutskie et al. 2006). In the following sections we describe the photometry used for each SN sibling in this analysis. All of the photometric data detailed here have been compiled and are available online at <https://github.com/ariannadwomoh/SNIRS>.

#### 2.2.1. SN 1980N, SN 1981D, SN 2006dd, & SN 2006mr

This sibling set has four SNe within the host galaxy NGC 1316, as seen in Fig. 1. All SNe are Type Ia, with SN 2006mr (Monard & Folatelli 2006) being 91bg-like. The NIR photometry for SN 1980N (Maza & Wischnjewsky 1980) and SN 1981D (Cragg et al. 1981; Evans 1982) is given in Elias et al. (1981), and the observations in the  $JHK$ -bands were obtained using the Cerro Tololo Inter-American Observatory (CTIO) 4-meter and 1.5-meter telescopes. For SN 2006dd (Monard 2006),

<sup>1</sup> <https://www.wis-tns.org/>.

<sup>2</sup> <https://ned.ipac.caltech.edu/>.

**Table 1.** General information about each SN sibling

SN	Host Galaxy	Type	NIR Photometry Source	$z^a$	Bands	RA	DEC	Opt. Peak MJD	Epochs <sup>b</sup>
1980N		Ia	Elias et al. (1981)		<i>JH</i>	03:23:00.30	−37:12:50.00	44586.8(2)	27
1981D	NGC 1316	Ia	Elias et al. (1981)	0.006010(10)	<i>JH</i>	03:22:38.40	−37:13:58.00	44680.5(2)	14
2006dd		Ia	Stritzinger et al. (2010)		<i>JH</i>	03:22:41.62	−37:12:13.00	53919.5(1)	44
2006mr		91bg-like	Contreras et al. (2010)		<i>JH</i>	03:22:42.84	−37:12:28.51	54050.4(1)	59
2002bo	NGC 3190	Ia	Benetti et al. (2004)	0.004370(13)	<i>JH</i>	10:18:06.51	+21:49:41.70	52356.0(2)	10
2002cv		Ia	Elias-Rosa et al. (2008)		<i>JH</i>	10:18:03.68	+21:50:06.00	52419.6(7) <sup>c</sup>	27
2002dj	NGC 5018	Ia	Pignata et al. (2008)	0.009393(30)	<i>JH</i>	13:13:00.34	−19:31:08.69	52451.1(1)	42
2021fxy		Ia	DEHVILS		<i>YJH</i>	13:13:01.57	−19:30:45.18	59306.1(2)	18
2007on	NGC 1404	Ia	CSP	0.006494(13)	<i>YJH</i>	03:38:50.90	−35:34:30.00	54420.5(1)	155
2011iv		Ia	CSP		<i>YJH</i>	03:38:51.35	−35:35:31.99	55905.3(1)	58
2011at	MCG -2-24-27	Ia	CfA	0.006758(2)	<i>JH</i>	09:28:57.56	−14:48:20.59	55635.0(50) <sup>d</sup>	27
2020jgl		Ia	DEHVILS		<i>YJH</i>	09:28:58.43	−14:48:19.88	58993.0(3)	15
2020sjo	NGC 1575	Ia	DEHVILS	0.031265(21)	<i>YJH</i>	04:26:21.95	−10:05:55.72	59107.6(2)	20
2020zhh		Ia	DEHVILS		<i>YJH</i>	04:26:19.84	−10:05:56.86	59178.4(2)	3

NOTE—

<sup>a</sup> Heliocentric redshift of the host galaxy from NED.<sup>b</sup> Total number of NIR observations in the bandpasses used in this analysis. Each filter is counted separately.<sup>c</sup> We fit for the optical peak MJD for this SN finding 52418.1(2) with SALT3-NIR and 52419.1(1) with SNooPy.<sup>d</sup> We fit for the optical peak MJD for this SN finding 55631.3(6) with SALT3-NIR and 55628.2(4) with SNooPy.

Stritzinger et al. (2010) obtained their photometry at CTIO using the SMARTS 1.3-meter telescope equipped with A Novel Double-Imaging CAMera (ANDICAM) and a small portion of the data with the Swope telescope and RetroCam imager as a part of CSP in the  $JHK_s$ -bands. Contreras et al. (2010) used the Irene du Pont (du Pont) 2.5-meter telescope with the Wide Field IR Camera (WIRC) to obtain photometry for SN 2006mr in the  $YJH$ -bands.

$JHK_s$  magnitudes for SN 2006dd were calibrated directly to the Persson et al. (1998) NIR photometric system. Similar to SN 2006dd, the local NIR sequence for SN 2006mr was calibrated to the Persson et al. (1998) system. Elias et al. (1981) state that the observations for both SN 1980N and SN 1981D are on the natural  $JHKL$  system of their respective observatories.

### 2.2.2. SN 2002bo & SN 2002cv

This sibling pair, SN 2002bo (Cacella et al. 2002) and SN 2002cv (Larionov et al. 2002), is located within NGC 3190. The NIR data for SN 2002bo, as detailed in Benetti et al. (2004), were obtained using the 1.55-meter Carlos Sanchez Telescope with the CAIN infrared camera as well as the 2.5-meter Nordic Optical Telescope (NOT) with the NOTCam infrared camera in the  $JHK_s$ -bands. SN 2002cv NIR data in the  $JHK_s$ -bands were found using the 1.08-meter AZT-24 Telescope along

with SWIRCAM and the 3.6-meter European Southern Observatory New Technology Telescope (ESO-NTT) equipped with the Son of ISAAC (Sofi) camera, as noted in Elias-Rosa et al. (2008).

For SN 2002bo, all observations are calibrated using NOTCam images and the photometric standards stated in Hunt et al. (1998) and Persson et al. (1998). The calibration of SN 2002cv data was derived using two local stars.

Of note, we use the more tightly constrained value for the optical peak MJD value for SN 2002bo from Krisciunas et al. (2004b) with an uncertainty of 0.2 days rather than that from Benetti et al. (2004) in Table 1. Additionally, since SN 2002cv was not observable in the  $B$ -band, Elias-Rosa et al. (2008) report an  $I$ -band maximum of  $\text{MJD} = 52414.6 \pm 0.2$ . We make an initial estimate for  $B$ -band maximum as approximately 5 days later than  $I$ -band maximum and incorporate extra uncertainty on the value. Because of this, we fit for a time of maximum when fitting the LC from SN 2002cv.

### 2.2.3. SN 2002dj & SN 2021fxy

We obtain NIR photometric data in the  $JH$ - and  $YJH$ -bands for SN 2002dj (Hutchings & Li 2002) and SN 2021fxy (Itagaki 2021), found in NGC 5018 (DerKacy et al. 2023), from Pignata et al. (2008) and DEHVILS, respectively. For SN 2002dj, the NIR data

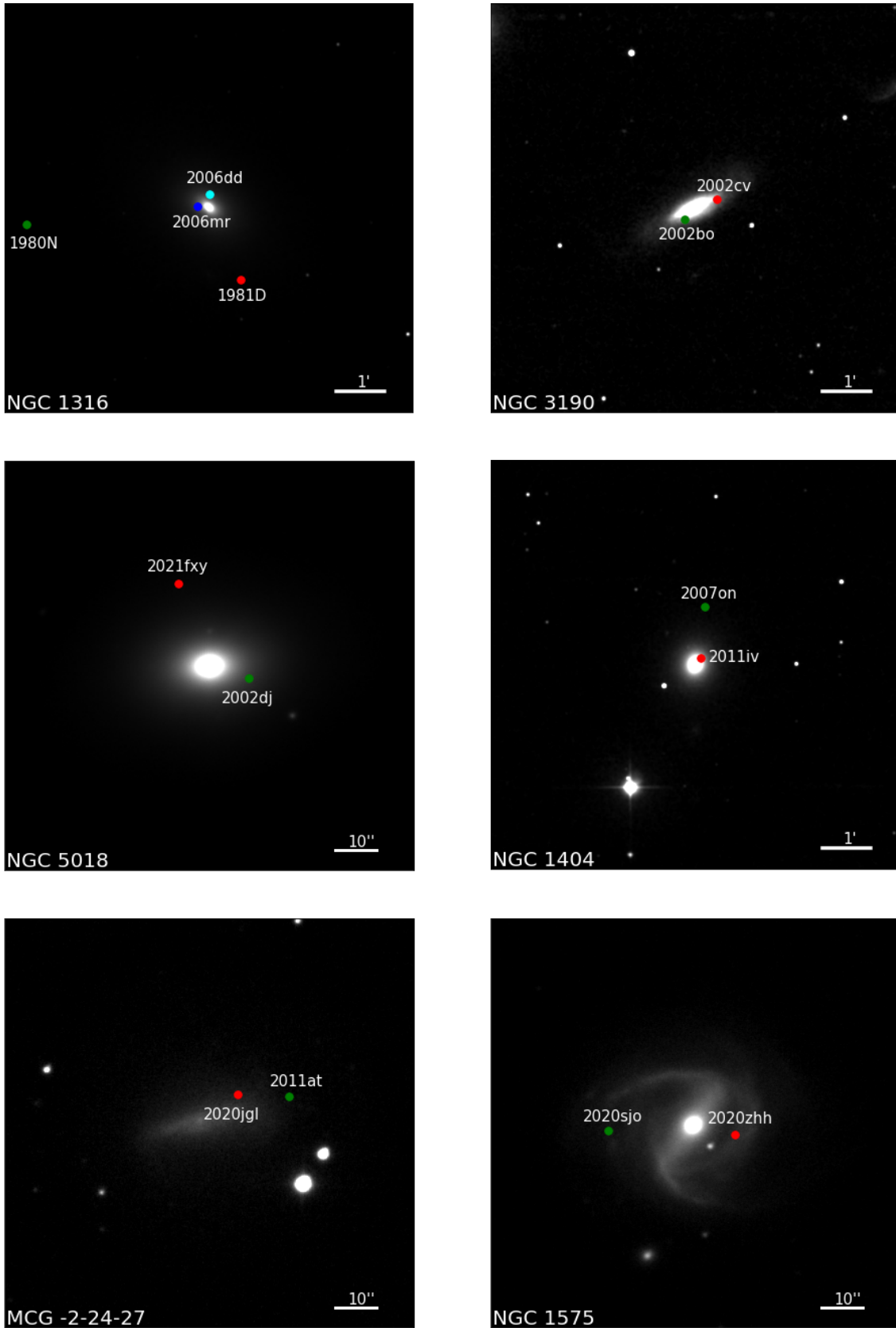


**Figure 1.** Images of the six SN sibling host galaxies. The colored markers indicate the locations of the SNe. All images are in *J*-band, and North is up and East is to the left for each image.



were obtained using the 1.0-meter telescope at CTIO equipped with ANDICAM and ESO-NTT equipped with SofI. For SN 2021fxy, the Wide Field CAMera (WFCAM) mounted onto the 3.8-meter United Kingdom Infrared Telescope (UKIRT) was used.

NIR data reductions for SN 2002dj were carried out using standard Image Reduction and Analysis Facility (IRAF) routines. An illumination correction was applied to all SofI images and four stars close to SN 2002dj were calibrated in the  $JHK_s$ -bands using the Persson et al. (1998) system. For the calibration of SN 2021fxy, and for all other DEHVILS SNe, Peterson et al. (2023) do a transformation of 2MASS magnitudes to WFCAM magnitudes which are further calibrated using Hubble Space Telescope CALSPEC stars.

#### 2.2.4. SN 2007on & SN 2011iv

The next pair of siblings are located in NGC 1404, and they are SN 2007on (Pollas & Klotz 2007) and SN 2011iv (Drescher et al. 2011). All NIR data in the  $YJH$ -bands were detailed in Gall et al. (2018) as a part of CSP. NIR imaging of SN 2007on was taken using the Swope telescope using RetroCam and the du Pont telescope with WIRC. As for SN 2011iv, data were collected using the du Pont telescope with RetroCam.

Gall et al. (2018) state that the  $JH$ -band values were calibrated to the Persson et al. (1998) system while the  $Y$ -band was calibrated to standard  $Y$ -band magnitudes computed using stellar atmosphere models (Castelli & Kurucz 2003) along with the Persson et al. (1998) system, as done in Hamuy et al. (2006).

#### 2.2.5. SN 2011at & SN 2020jgl

SN 2011at (Cox et al. 2011) and SN 2020jgl (Tonry et al. 2020) were found in MCG -2-24-27. Friedman et al. (2015) used the 1.3-meter Peters Automated Infrared Imaging TELEscope (PAIRITEL) at the Fred Lawrence Whipple Observatory to obtain  $JHK_s$ -band data for SN 2011at with CfA. Peterson et al. (2023) state that the NIR data for SN 2020jgl were obtained in the  $YJH$ -bands using WFCAM with DEHVILS.

PAIRITEL’s photometric observations for SN 2011at are calibrated with the 2MASS field star observations. SN 2020jgl LC data are from DEHVILS, and they are calibrated as such. Of note, there is no optical data and the NIR data obtained for SN 2011at covers only the secondary maximum of the LC (all data are  $\gtrsim 10$  days past optical maximum). Because of this, we fit for a time of maximum when fitting the LC from SN 2011at.

#### 2.2.6. SN 2020sjo & SN 2020zhh

All NIR data for the siblings SN 2020sjo (Perley & Sollerman 2020) and SN 2020zhh (Chambers et al.

2020), which are located in NGC 1575, were noted in Peterson et al. (2023) and obtained in the  $YJH$ -bands using WFCAM.

Since both siblings are from DEHVILS, they are calibrated in the same way with 2MASS and a refinement from CALSPEC stars.

### 3. DATA ANALYSIS

#### 3.1. Light Curve Fits

We use the SuperNova ANALysis (SNANA) software package to both fit and simulate SN Ia LCs (Kessler et al. 2009). In order to measure the distance to each SN, we fit LCs using both the Spectral Adaptive Light curve Template (SALT3-NIR; Kenworthy et al. 2021; Pierel et al. 2022) and SuperNova object oriented Python (SNooPy; Burns et al. 2011, 2014) EBV\_model2 LC models. With the exception of SN LCs from CSP and DEHVILS, which have well understood photometric systems, almost every SN LC is obtained with a different telescope and instrument. Due to the challenge of deducing the filter functions used and the likelihood that all data were transformed to a similar 2MASS system, we treat each photometric system as if it were that from 2MASS. As discussed in Appendix A, this is because we find that the calibration of the stellar observations around each SN is relatively consistent with the 2MASS system. While the range of median magnitude residuals is from  $-0.045$  to  $0.130$  mag, the median difference between 2MASS photometry and all other stellar photometry compiled is  $0.008$  mag.

SALT3-NIR fits from all six sets of siblings are presented in Fig. 2, and SNooPy fits are presented in Fig. 3. Fits to the data are capped at 50 days past optical peak, and the peak MJD value is fixed to the optical peak value for each SN given in Table 1 (with the exceptions of SN 2002cv and SN 2011at where we fit for the time of maximum because their peaks are both ill-constrained). All fits from SALT3-NIR have both the stretch parameter,  $x_1$ , and color parameter,  $c$ , fixed to zero (discussed further in Section 3.2) such that each SN NIR LC is treated as a standard candle, only the scaling parameter  $x_0$  is fit, and each  $\mu$  value is given by,

$$\mu = m_B - \mathcal{M}, \quad (1)$$

where  $m_B = -2.5 \log(x_0) + const.$  and  $\mathcal{M}$  is the globally fit absolute peak magnitude derived for the set of SNe and is fixed as a single value for all siblings.

SNooPy fits, on the other hand, incorporate stretch and color corrections. SNooPy’s stretch parameter,  $s_{BV}$ , and  $A_V$  are fit for in all cases except in extreme cases such as fast-declining ( $s_{BV} < 0.7$ ) or highly-extincted ( $A_V > 5.0$  mag) events because SNANA

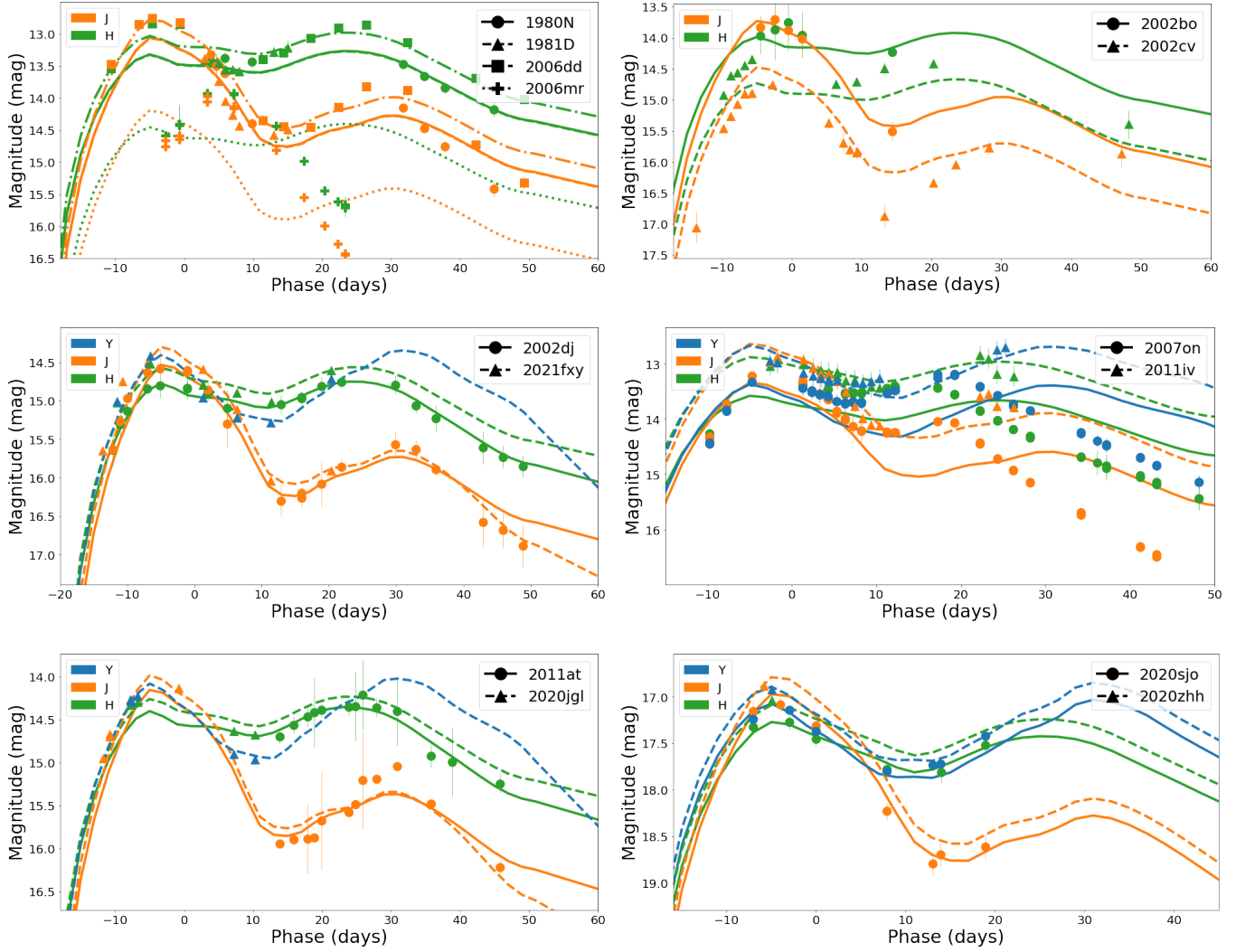


**Figure 2.** LC fits for each sibling set in our sample using SALT3-NIR. Phase is given with respect to optical peak. Each subplot features a specific marker and line style for every SN. The band colors are the same for all SNe and all panels.

SNooPy minimization fails at these levels. For example, for SN 2002cv, we fix  $A_V$  to the derived value of 8.4 mag reported in [Elias-Rosa et al. \(2008\)](#), and for SN 2011iv and SN 2007on, we fix  $s_{BV}$  to the reported values of 0.64 and 0.57, respectively, from [Gall et al. \(2018\)](#).

### 3.2. $\mu$ Comparisons

We provide a list of all  $\mu$  values from both SALT3-NIR and SNooPy in Table 2. The uncertainties in distance moduli do not include expected uncertainty from intrinsic scatter, as this is a parameter we aim to measure. With six sets of siblings, one of which is a set of four SNe and five of which are sibling pairs, this provides 11 potential  $\mu$  comparisons. Although [Hoogendam et al. \(2022\)](#) demonstrate that two 91bg-like siblings provide consistent  $\mu$  estimates, we find, like [Stritzinger et al. \(2010\)](#), that the derived distance modulus from

SN 2006mr is much larger than the other three siblings in NGC 1316. [Burns et al. \(2018\)](#) find consistency between the distance moduli of SN 2006mr and its siblings, reporting an  $s_{BV}$  value of 0.26. However, we are unable to recover a  $\mu$  value for SN 2006mr that is within 0.5 mag of its siblings even when we fix  $s_{BV}$  to this value. Thus, we do not include SN 2006mr in our sample of  $\mu$  comparisons. This reduces the total number of  $\mu$  comparisons to eight. We plot this final sample comparing the  $\mu$  values between siblings in Fig. 4.  $\mu$  uncertainties do not include expected uncertainty from intrinsic scatter, and SALT3-NIR  $\mu$  uncertainties are smaller than those from SNooPy in large part because they do not include uncertainties due to stretch and color corrections.

Using the SALT3-NIR model, we find a median absolute difference for the eight siblings  $\mu$  comparisons of 0.248 mag and a range of absolute differences from

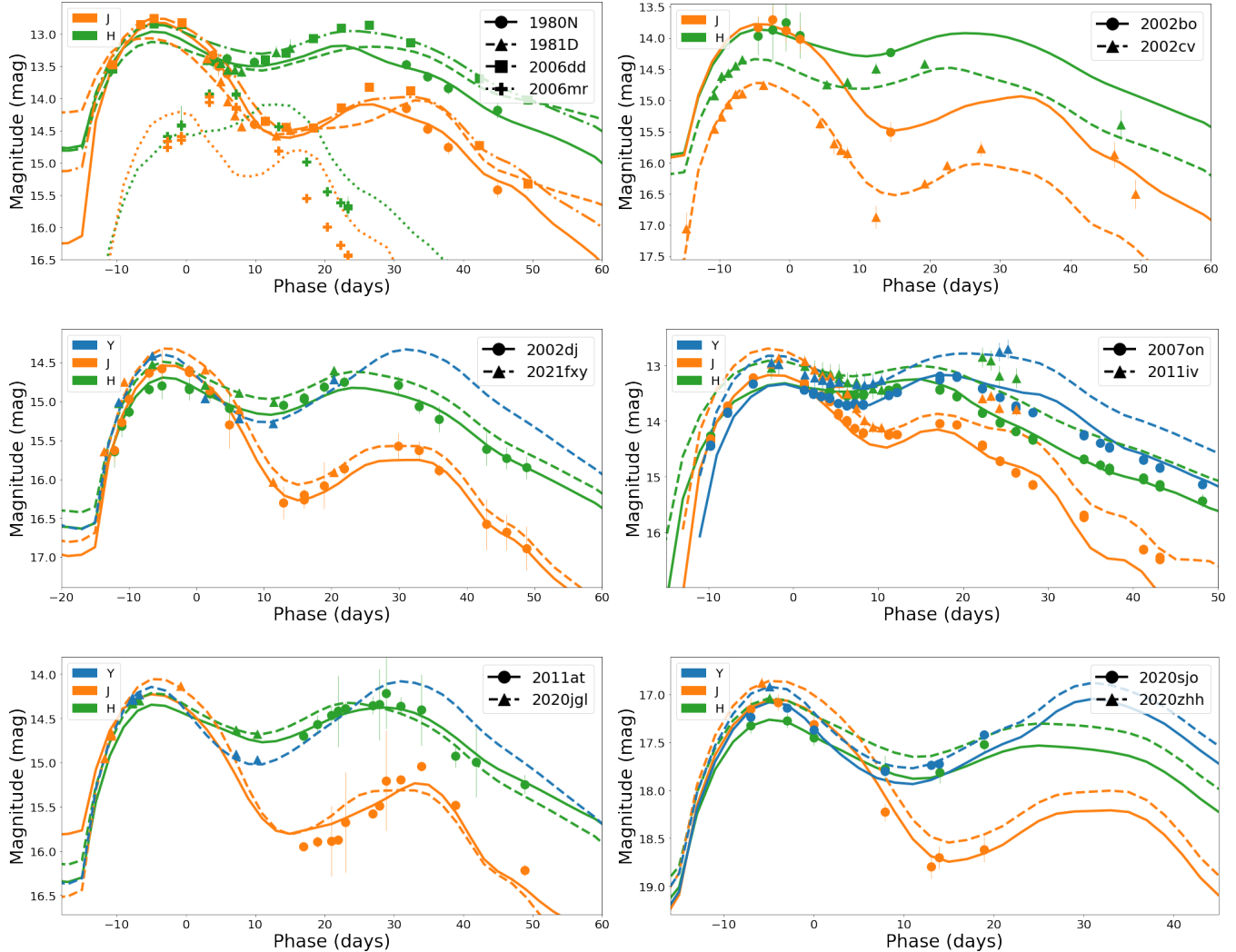


**Figure 3.** Similar to Fig. 2 but with LC fits using SNOOPy.

0.007 to 0.747 mag. Using the SNOOPy model, we find a median absolute difference of 0.186 mag and a range from 0.001 to 0.295 mag. As can be seen from Fig. 2, the SN 2002cv and SN 2002bo pair have poor LC fits from SALT3-NIR which are slightly improved when using SNOOPy. This pair also corresponds to the largest  $\mu$  residual of 0.747 mag from SALT3-NIR. The SNOOPy fits result in more consistent  $\mu$  values between siblings than the SALT3-NIR fits, however, we recognize that the SNOOPy fits incorporate fits to stretch and color parameters while the SALT3-NIR fits do not.

When calculating SALT3-NIR fits, we fix both  $x_1$  and  $c$  to zero, treating the SNe as standard candles. When attempting to fit for stretch and color parameters with SALT3-NIR and NIR data alone, the fits are unable to be constrained using SNANA. Furthermore, we cannot use optically-fitted  $x_1$  and  $c$  parameters because optical data are not available for all SNe in our sample. When we

try fixing  $A_V = 0$  mag and  $s_{BV} = 1$  with SNOOPy, rather than fitting for  $A_V$  and  $s_{BV}$ , in a similar fashion to fixing both  $x_1$  and  $c$  for SALT3-NIR, we find that the SNOOPy fits become worse and the differences in  $\mu$  values between siblings increase; the median absolute difference in  $\mu$  values goes from 0.186 mag to 0.279 mag.

Distance moduli using NIR data for some pairs of SN siblings have been analyzed previously in the literature. Stritzinger et al. (2010) report the range of differences in distance modulus is 0.236 mag for SN 1980N, SN 1981D, and SN 2006dd using SNOOPy and NIR data alone, with SN 2006dd having the smallest  $\mu$  value, and Gall et al. (2018) report a difference in  $\mu$  values of 0.40 mag for SN 2007on and SN 2011iv (with SN 2007on having the larger  $\mu$  value) using SNOOPy and optical+NIR data and 0.20 mag with  $H$ -band alone. Results from our analysis are in agreement with these findings, particularly when using SNOOPy. For SN 1981D, SN 1980N, and

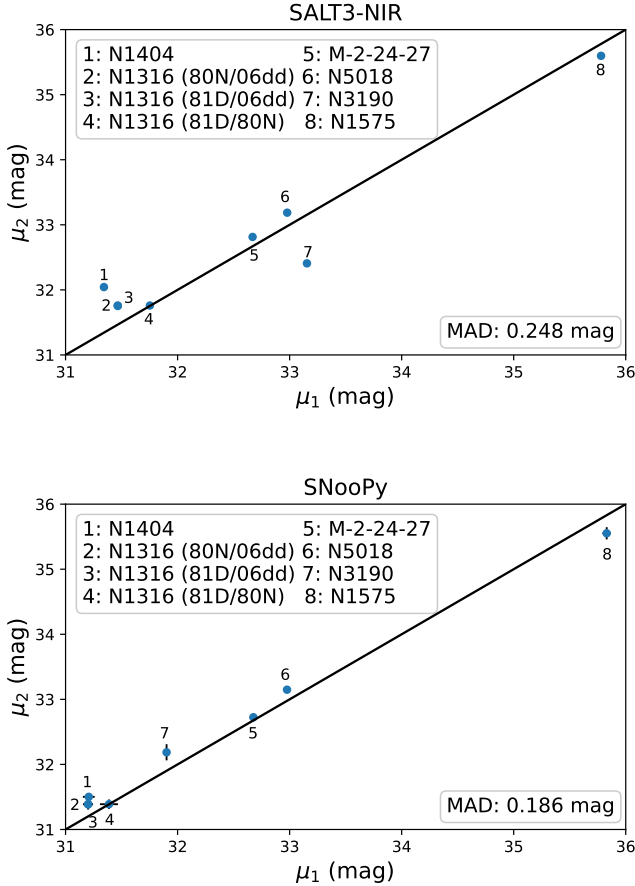


**Figure 4.** Comparing measured  $\mu$  values obtained from both LC fitting models.  $\mu_1$  represents one sibling in the pair and  $\mu_2$  represents the other — either sibling could be on either axis. The black diagonal line represents  $y = x$ . Each pair is labeled with a number and indicated in the legend. The median absolute difference (MAD) for each set is also given. The uncertainties shown do not include intrinsic scatter.

SN 2006dd, our  $\mu$  values span 0.188 mag when using SNooPy and SN 2006dd results in the smallest  $\mu$  value as well. For SN 2007on and SN 2011iv, we find a difference in  $\mu$  values of 0.30 mag and SN 2007on demonstrates the larger  $\mu$  value.

#### 4. COMPARISON TO SIMULATIONS

To estimate agreement between SN siblings, we find LCs from a simulated sample of SNe Ia which have similar redshift values, within 0.005 in redshift, and compare the results to our sample’s results following Scolnic et al. (2020). We construct these simulations of NIR LCs following Peterson et al. in prep. who use SNANA to generate accurate simulations based on characteristics from DEHVILS survey data such as LC cadence, coverage, and quality. While our sample of SNe is only  $\sim 30\%$  from

**Table 2.** Resulting distances from SALT3-NIR and SNooPy for all siblings using NIR data.

SN Name	Host Galaxy	$\mu_{\text{SALT3-NIR}}$	$\mu_{\text{SNooPy}}$
1980N		31.753(27)	31.387(80)
1981D	NGC 1316	31.759(28)	31.389(73)
2006dd		31.466(22)	31.201(44)
2006mr		32.889(19)	33.039(100)
2002bo	NGC 3190	32.408(47)	32.186(124)
2002cv		33.155(24)	31.902(22)
2002dj	NGC 5018	33.187(19)	33.148(44)
2021fxy		32.978(26)	32.977(31)
2007on	NGC 1404	32.043(10)	31.502(32)
2011iv		31.343(17)	31.207(53)
2011at	MCG -2-24-27	32.813(24)	32.724(62)
2020jgl		32.669(30)	32.676(32)
2020sjo	NGC 1575	35.780(22)	35.830(38)
2020zhh		35.597(56)	35.552(94)

DEHVILS, these simulations provide a baseline set of LCs from which we can choose LCs with similar redshifts as the LCs from our sample. To evaluate the amount of intrinsic scatter present in our sample, simulations are created both with and without intrinsic scatter included (0.14 mag). This scatter is modeled as achromatic, similar to that done for the optical in Guy et al. (2010). All simulated LCs are fit using SALT3-NIR with both  $x_1$  and  $c$  fixed to zero. Given that minimal work has been done on creating simulations following the SNooPy model, we use the SALT3-NIR model here in this work for the construction of simulations, however we encourage future works to incorporate SNooPy simulations.

We construct our first simulation, including intrinsic scatter, totaling 26,533 LCs. From this, we compile 1,000 sets of eight differences in  $\mu$  values where each of the  $\mu$  values (corrected to be at the same redshift) are selected at random from the sample of simulated SNe with redshift values within 0.005 of each of our SN siblings’ redshift values. We present a histogram of the median absolute differences in  $\mu$  values for those 1,000 sets of eight differences in  $\mu$  values in Fig. 5 in blue, and indicate the median absolute difference from SALT3-NIR for our sample as a dotted black vertical line. If there were agreement between our sample’s median absolute difference and the simulation median absolute differences in  $\mu$  values, the line in Fig. 5 would lie closer to the peak of the blue histogram. In the figure, we can see that our data value lies on the right side. 2.7% of this sample has differences greater than the differences in our data sample. The standard deviation of the median absolute



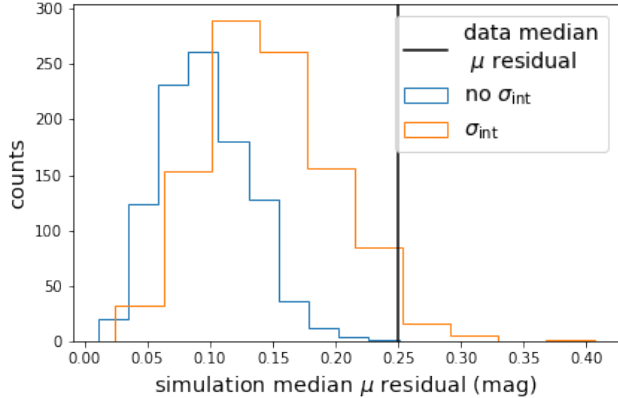


**Figure 5.** Each histogram features statistics from 8,000 random simulation differences in  $\mu$  residuals obtained from lists of SNe that have redshift values within 0.005 of each of our SN siblings. The blue histogram includes simulated data with  $\sigma_{\text{int}}$  while the orange histogram does not include  $\sigma_{\text{int}}$ . One count on this histogram is the median of the list of eight simulated differences in  $\mu$  residuals. 99.9% of simulated sample without  $\sigma_{\text{int}}$  has differences lower than our differences while 97.3% of the simulated sample with  $\sigma_{\text{int}}$  has differences lower than our differences. Our differences are represented by the vertical dotted line.

differences in  $\mu$  values from this simulation, with intrinsic scatter, of 0.052 mag provides an estimate for uncertainty on the median absolute differences in  $\mu$  values in our analysis.

We then make another simulation in which we do not include intrinsic scatter, which can be seen as the dotted orange histogram in Fig. 5. The peak of the orange histogram falls to the left of the sample with intrinsic scatter, as expected, and we find the resulting median absolute difference in  $\mu$  values from our sample to be even more unlikely if intrinsic scatter were not present in SNe Ia. Approximately 0.1% of the simulated values, not accounting for intrinsic scatter, have differences greater than the differences in our data sample. *We can now show from this SN siblings analysis, with high significance, that there must be intrinsic scatter present in the NIR that cannot be attributed to host galaxy properties.*

## 5. DISCUSSION AND CONCLUSION

We perform a complete literature search of all SNe discovered and find six sets of SN siblings with NIR data. Of these six sibling sets, one set includes four SNe (three of which are Type Ia-normal), and one SN LC fails quality cut criteria. This results in a total of eight pairs of SN siblings with median absolute differences in  $\mu$  values of 0.248 mag and 0.186 mag when fitting with SALT3-NIR and SNooPy, respectively. Utilizing simulations, we find

SN siblings seem to be no closer in terms of  $\mu$  than two random SNe at the same redshift. When the simulations do not include intrinsic scatter, recovering differences of the same scale becomes even more unlikely, occurring only 0.1% of the time. While we do not attribute all of the scatter observed in the data to  $\sigma_{\text{int}}$ , this finding supports the existence of intrinsic scatter in the NIR.

With predominantly optical data alone, Burns et al. (2020) report a level of consistency in distance of  $\sim 3\%$ ; for our NIR sample, we report approximately 9% consistency in distance. To better understand this discrepancy, we obtain optical-only LCs from ATLAS and Pantheon+ for six out of eight pairs of siblings used in this analysis which, when fit with SALT3 and fitting for  $x_1$  and  $c$ , have a median absolute difference in  $\mu$  values of 0.177 mag. The median absolute differences from the same set of six pairs with NIR-only LCs are 0.248 mag and 0.186 mag from using SALT3-NIR and SNooPy, respectively. While the optical data present smaller differences in  $\mu$  values between siblings, it is possible that this difference is due to the low statistics, data quality, and data reduction of this NIR sample.

One interesting finding about the SALT3-NIR model (Pierel et al. 2022) is that even though the photometric data demonstrate that there are SNe that decline quickly even in the NIR, modifying the “stretch” parameter  $x_1$  (which is defined in the optical) does not result in reasonable fits for fast-declining NIR LCs. This inability to fit fast-declining NIR LCs is most evident for SN 2007on where the characteristic secondary maximum in the NIR begins  $\lesssim 20$  days past NIR maximum as compared to the more typical  $\sim 30$  days past NIR maximum (Dhawan et al. 2015; Mandel et al. 2022). Further, as can be seen from figure 7 in Pierel et al. (2022), modifying SALT3  $x_1$  does not change the phase of any of the LC features for  $J$ - or  $H$ -band significantly at all. In contrast, SNooPy’s  $s_{BV}$  parameter does act as a “stretch” parameter in the NIR and by fixing  $s_{BV} = 0.57$  as derived by Gall et al. (2018), we obtain a reasonable fit to the LC of SN 2007on from SNooPy.

In this analysis, we fix both  $x_1$  and  $c$  when using SALT3-NIR. When we attempt to fit for  $x_1$  and  $c$  using SALT3-NIR and NIR data alone, SNANA is unable to produce LC fits for half of the SNe. All other SN LCs successfully fit by SNANA result in either unreasonable  $x_1$  or  $c$  parameters ( $|x_1| > 3$ ,  $|c| > 0.3$ ) or unreasonable uncertainties on those parameters ( $\sigma_{x_1} > 1$ ,  $\sigma_c > 0.1$ ).

We encourage further analysis into NIR LC models not just for SALT3-NIR, but also for SNooPy. Particularly, we believe improvements could be made in fitting the secondary maximum since we find the secondary maxima in our sample to be fit relatively poorly (e.g.,

SN 2011iv, SN 2002dj, SN 2002cv). We expect improvements could be made by adding to the training samples for both SALT3-NIR and SNooPy and specifically adding SNe with quality coverage of both the primary and secondary maxima across a large phase range. Interestingly, in the case of SN 2011at, which only has NIR data covering the secondary maximum, the LC fits well and the  $\mu$  value is consistent with that from SN 2020jgl (only a 0.05 mag difference) indicating potential for measuring distances with NIR LCs even if the primary maximum is missed.

With the Roman space telescope (Spiegel et al. 2015; Hounsell et al. 2018; Rose et al. 2021),  $\sim 1,300$  SNe will be observed in the first two years with rest frame NIR data (Peterson et al. in prep.). Given that Scolnic et al. (2020) report eight sibling pairs out of  $\sim 3,000$  SNe, we can expect approximately 3–4 more NIR sibling pairs from Roman. This is not a sizeable increase in statistics, but it will be an interesting cross-check for Roman nonetheless. Additionally, if we search through NIR samples with larger statistics but less LC coverage, such as the Hawaii Supernova Flows survey (HSF; Do

et al. in prep.), we may find more siblings that could be used in a future NIR analysis. For now, the next step is to understand whether or not the advantages to SN observations in the NIR can be seen with SN siblings from a larger sample NIR LCs.

This research has made use of the NASA/IPAC Extragalactic Database (NED), which is funded by the National Aeronautics and Space Administration and operated by the California Institute of Technology. UKIRT is owned by the University of Hawaii (UH) and operated by the UH Institute for Astronomy. When (some of) the data reported here were obtained, the operations were enabled through the cooperation of the East Asian Observatory. D.S. is supported by Department of Energy grant DE-SC0010007, the David and Lucile Packard Foundation, the Templeton Foundation and Sloan Foundation. This research has made use of NASA’s Astrophysics Data System.

Software: **SNANA** (Kessler et al. 2009), **astropy** (Astropy Collaboration et al. 2013, 2018), **matplotlib** (Hunter 2007), **NumPy** (van der Walt et al. 2011)

## REFERENCES

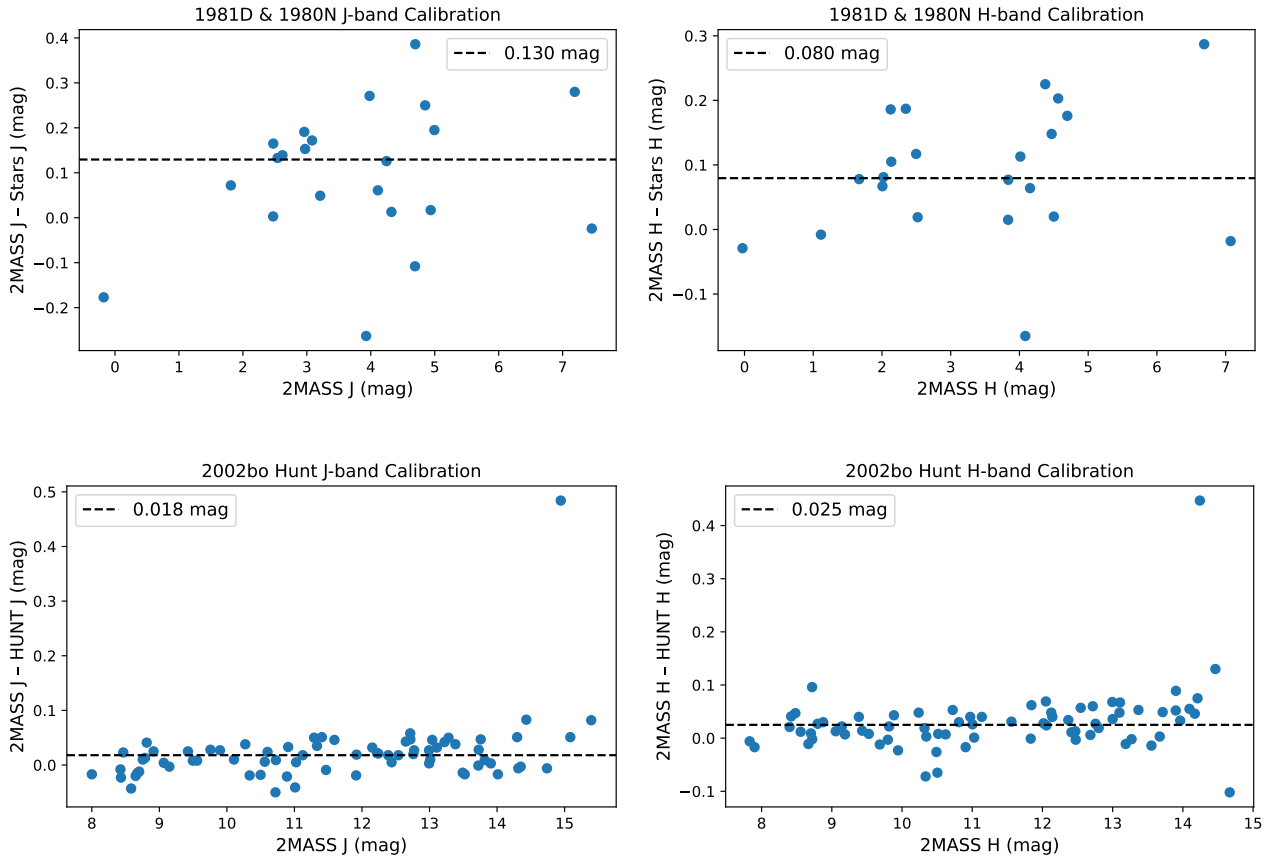
- Astropy Collaboration, Price-Whelan, A. M., Sipőcz, B. M., et al., 2018, *AJ*, 156, 3, 123, arXiv:1801.02634
- Astropy Collaboration, Robitaille, T. P., Tollerud, E. J., et al., 2013, *A&A*, 558, A33, arXiv:1307.6212
- Avelino, A., Friedman, A. S., Mandel, K. S., Jones, D. O., Challis, P. J., Kirshner, R. P., 2019, *ApJ*, 887, 1, 106, arXiv:1902.03261
- Barone-Nugent, R. L., Lidman, C., Wyithe, J. S. B., et al., 2012, *MNRAS*, 425, 2, 1007, arXiv:1204.2308
- Bellm, E. C., Kulkarni, S. R., Graham, M. J., et al., 2019, *PASP*, 131, 995, 018002, arXiv:1902.01932
- Benetti, S., Meikle, P., Stehle, M., et al., 2004, *MNRAS*, 348, 1, 261, arXiv:astro-ph/0309665
- Biswas, R., Goobar, A., Dhawan, S., et al., 2022, *MNRAS*, 509, 4, 5340, arXiv:2103.16978
- Brout, D., Scolnic, D., 2021, *ApJ*, 909, 1, 26, arXiv:2004.10206
- Brout, D., Scolnic, D., Popovic, B., et al., 2022, *ApJ*, 938, 2, 110, arXiv:2202.04077
- Burns, C. R., Ashall, C., Contreras, C., et al., 2020, *ApJ*, 895, 2, 118, arXiv:2004.13069
- Burns, C. R., Parent, E., Phillips, M. M., et al., 2018, *ApJ*, 869, 1, 56, arXiv:1809.06381
- Burns, C. R., Stritzinger, M., Phillips, M. M., et al., 2011, *AJ*, 141, 1, 19, arXiv:1010.4040
- Burns, C. R., Stritzinger, M., Phillips, M. M., et al., 2014, *ApJ*, 789, 1, 32, arXiv:1405.3934
- Cacella, P., Hirose, Y., Nakano, S., Kushida, Y., Kushida, R., Li, W. D., 2002, *IAUC*, 7847, 1
- Castelli, F., Kurucz, R. L., 2003, in *Modelling of Stellar Atmospheres*, edited by Piskunov, N., Weiss, W. W., Gray, D. F., vol. 210, A20, arXiv:astro-ph/0405087
- Chambers, K. C., Boer, T. D., Bulger, J., et al., 2020, *Transient Name Server Discovery Report*, 2020-3428, 1
- Contreras, C., Hamuy, M., Phillips, M. M., et al., 2010, *AJ*, 139, 2, 519, arXiv:0910.3330
- Cox, L., Newton, J., Puckett, T., et al., 2011, *Central Bureau Electronic Telegrams*, 2676, 1
- Cragg, T., Evans, R., Maza, J., 1981, *IAUC*, 3583, 1
- DerKacy, J. M., Paugh, S., Baron, E., et al., 2023, *MNRAS*, 522, 3, 3481, arXiv:2212.06195
- Dhawan, S., Leibundgut, B., Spyromilio, J., Maguire, K., 2015, *MNRAS*, 448, 2, 1345, arXiv:1502.00568
- Drescher, C., Parker, S., Brimacombe, J., Noguchi, T., Nakano, S., 2011, *Central Bureau Electronic Telegrams*, 2940, 1
- Elias, J. H., Frogel, J. A., Hackwell, J. A., Persson, S. E., 1981, *ApJL*, 251, L13
- Elias-Rosa, N., Benetti, S., Turatto, M., et al., 2008, *MNRAS*, 384, 1, 107, arXiv:0710.4503

- Evans, R., 1982, IAUC, 3697, 3
- Folatelli, G., Phillips, M. M., Burns, C. R., et al., 2010, AJ, 139, 1, 120, arXiv:0910.3317
- Freedman, W. L., Madore, B. F., Hatt, D., et al., 2019, ApJ, 882, 1, 34, arXiv:1907.05922
- Friedman, A. S., Wood-Vasey, W. M., Marion, G. H., et al., 2015, ApJS, 220, 1, 9, arXiv:1408.0465
- Gall, C., Stritzinger, M. D., Ashall, C., et al., 2018, A&A, 611, A58, arXiv:1707.03823
- Guy, J., Sullivan, M., Conley, A., et al., 2010, A&A, 523, A7, arXiv:1010.4743
- Hamuy, M., Folatelli, G., Morrell, N. I., et al., 2006, PASP, 118, 839, 2, arXiv:astro-ph/0512039
- Hoogendam, W. B., Ashall, C., Galbany, L., et al., 2022, ApJ, 928, 2, 103, arXiv:2109.14644
- Hounsell, R., Scolnic, D., Foley, R. J., et al., 2018, ApJ, 867, 1, 23, arXiv:1702.01747
- Hunt, L. K., Mannucci, F., Testi, L., et al., 1998, AJ, 115, 6, 2594, arXiv:astro-ph/9803153
- Hunter, J. D., 2007, Computing in Science and Engineering, 9, 3, 90
- Hutchings, D., Li, W. D., 2002, IAUC, 7918, 1
- Itagaki, K., 2021, Transient Name Server Discovery Report, 2021-785, 1
- Jones, D. O., Mandel, K. S., Kirshner, R. P., et al., 2022, ApJ, 933, 2, 172, arXiv:2201.07801
- Kasen, D., 2006, ApJ, 649, 2, 939, arXiv:astro-ph/0606449
- Kelsey, L., 2023, arXiv e-prints, arXiv:2303.02020, arXiv:2303.02020
- Kenworthy, W. D., Jones, D. O., Dai, M., et al., 2021, ApJ, 923, 2, 265, arXiv:2104.07795
- Kessler, R., Becker, A. C., Cinabro, D., et al., 2009, ApJS, 185, 1, 32, arXiv:0908.4274
- Krisciunas, K., Phillips, M. M., Suntzeff, N. B., 2004a, ApJL, 602, 2, L81, arXiv:astro-ph/0312626
- Krisciunas, K., Suntzeff, N. B., Phillips, M. M., et al., 2004b, AJ, 128, 6, 3034, arXiv:astro-ph/0409036
- Larionov, V., Arkharov, A., Caratti o Garatti, A., et al., 2002, IAUC, 7901, 1
- Mandel, K. S., Thorp, S., Narayan, G., Friedman, A. S., Avelino, A., 2022, MNRAS, 510, 3, 3939, arXiv:2008.07538
- Mandel, K. S., Wood-Vasey, W. M., Friedman, A. S., Kirshner, R. P., 2009, ApJ, 704, 1, 629, arXiv:0908.0536
- Maza, J., Wischnjewsky, M., 1980, IAUC, 3548, 1
- Meikle, W. P. S., 2000, MNRAS, 314, 4, 782, arXiv:astro-ph/9912123
- Monard, L. A. G., 2006, Central Bureau Electronic Telegrams, 553, 1
- Monard, L. A. G., Folatelli, G., 2006, Central Bureau Electronic Telegrams, 723, 1
- Perley, D., Sollerman, J., 2020, Transient Name Server Discovery Report, 2020-2703, 1
- Persson, S. E., Murphy, D. C., Krzeminski, W., Roth, M., Rieke, M. J., 1998, AJ, 116, 5, 2475
- Peterson, E. R., Jones, D. O., Scolnic, D., et al., 2023, MNRAS, 522, 2, 2478, arXiv:2301.11868
- Phillips, M. M., 2012, PASA, 29, 4, 434, arXiv:1111.4463
- Pierel, J. D. R., Jones, D. O., Kenworthy, W. D., et al., 2022, ApJ, 939, 1, 11, arXiv:2209.05594
- Pignata, G., Benetti, S., Mazzali, P. A., et al., 2008, MNRAS, 388, 3, 971, arXiv:0805.1089
- Pollas, C., Klotz, A., 2007, Central Bureau Electronic Telegrams, 1121, 1
- Riess, A. G., Yuan, W., Macri, L. M., et al., 2022, ApJL, 934, 1, L7, arXiv:2112.04510
- Rose, B. M., Baltay, C., Hounsell, R., et al., 2021, arXiv e-prints, arXiv:2111.03081, arXiv:2111.03081
- Scolnic, D., Brout, D., Carr, A., et al., 2022, ApJ, 938, 2, 113, arXiv:2112.03863
- Scolnic, D., Smith, M., Massiah, A., et al., 2020, ApJL, 896, 1, L13, arXiv:2002.00974
- Skrutskie, M. F., Cutri, R. M., Stiening, R., et al., 2006, AJ, 131, 2, 1163
- Spergel, D., Gehrels, N., Baltay, C., et al., 2015, arXiv e-prints, arXiv:1503.03757, arXiv:1503.03757
- Stritzinger, M., Burns, C. R., Phillips, M. M., et al., 2010, AJ, 140, 6, 2036, arXiv:1009.4390
- Tonry, J., Denneau, L., Heinze, A., et al., 2020, Transient Name Server Discovery Report, 2020-1250, 1
- Tonry, J. L., Denneau, L., Heinze, A. N., et al., 2018, PASP, 130, 988, 064505, arXiv:1802.00879
- van der Walt, S., Colbert, S. C., Varoquaux, G., 2011, Computing in Science and Engineering, 13, 2, 22, arXiv:1102.1523
- Ward, S. M., Thorp, S., Mandel, K. S., et al., 2022, arXiv e-prints, arXiv:2209.10558, arXiv:2209.10558
- Wood-Vasey, W. M., Friedman, A. S., Bloom, J. S., et al., 2008, ApJ, 689, 1, 377, arXiv:0711.2068

## APPENDIX

## A. PHOTOMETRIC CALIBRATION ANALYSIS

Here, we ensure the calibration of the data is relatively consistent and accurate enough for use in our analysis. We do this by comparing the individual band magnitudes from stellar photometry to 2MASS magnitudes. In Fig. 6, each subfigure features a residual mag vs. mag plot. These plots show the difference between the 2MASS stellar magnitudes and the respective magnitudes noted in the respective paper as a function of magnitude. The black dotted lines are the median of those residuals, which is given in the legend of each subfigure. To remove outliers, we placed a cut requiring the absolute value of the residuals to be  $< 0.5$  mag. The median of all the residuals combined is 0.008 mag. Additionally, the range of median magnitude residuals is from  $-0.045$  to 0.130 mag. When we do not consider the largest of the median magnitude residuals of 0.130 mag and 0.080 mag from comparing stellar photometry taken over 40 years ago to 2MASS, the range of median magnitude residuals goes from  $-0.045$  to 0.025 mag. If we take this offset into account by adding  $\sim 0.1$  mag to the  $\mu$  values obtained for SN 1980N and SN 1981D, this actually increases the difference between the  $\mu$  values of these SNe and that of SN 2006dd.



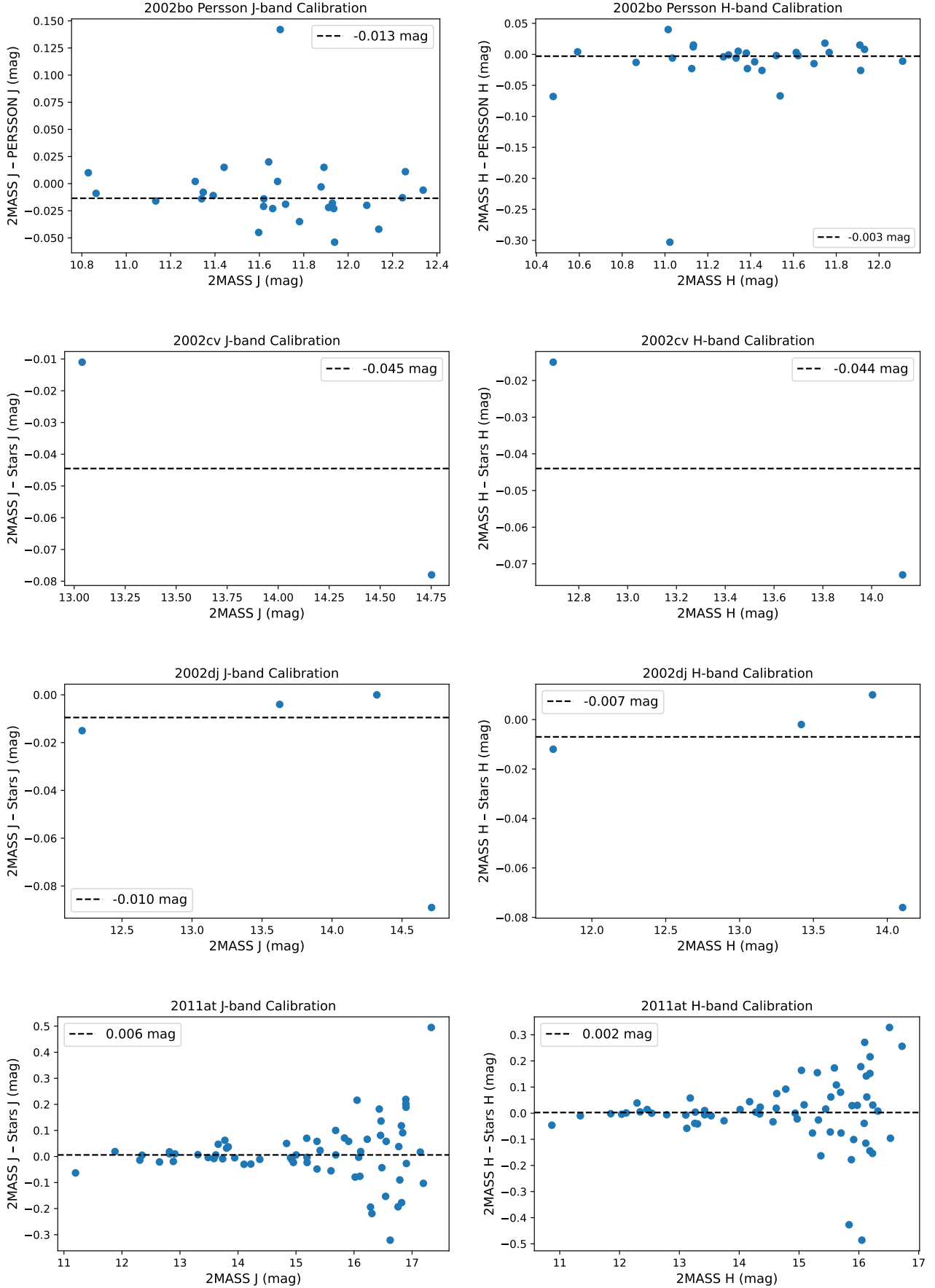


**Figure 6.** Magnitude residuals versus magnitude plots comparing sets of stellar photometry for each SN sibling to 2MASS photometry.